

**Cell, Volume 138**

## **A Systems-Level Analysis of Perfect**

### **Adaptation in Yeast Osmoregulation**

Dale Muzzey, Carlos A. Gómez-Uribe, Jerome T. Mettetal, and Alexander van Oudenaarden

#### **Glycerol Assays**

DMY034 cells were grown overnight in 100 ml selective minimal media. Log-phase cultures were split and supplemented either with PP1 (1-NM-PP1, EMD Biosciences) in DMSO or the same volume of DMSO alone. After 30 minutes, 1.17 g NaCl crystals were dissolved in each 50 ml culture such that [NaCl] rose by 0.4 M; this approach changed only the salt concentration, diluting neither cells nor media. At each time point (0, 15, 30, 60 minutes) relative to the addition of salt, three samples were collected: 100  $\mu$ l for cell density, 200  $\mu$ l for the “total” glycerol measurement, and 10 ml that yields both the “external” and “internal” measurements. Between sample collections, flasks were shaking at 225 rpm and 30°C.

To account for changes in cell density throughout the experiment, the OD<sub>600</sub> was measured on a sample containing cell culture and fresh water in the ratio 1:10; because salt-shock affects cell volume, we diluted cells in water to ensure that the volumes of salt-shocked and unshocked cells were roughly comparable.

The 200  $\mu$ l sample harvested for the “total” glycerol measurement was incubated at 95°C for 10 minutes and then spun at 13000 rpm for 3 minutes to pellet cell debris. A sample of the supernatant was added directly to the Free Glycerol Reagent Kit (Sigma) as

directed and then the OD<sub>540</sub> was measured. The reported per-cell glycerol measurements are in units of OD<sub>540</sub>/OD<sub>600</sub>.

The 10 ml sample was first spun at 2000 rpm for 2 minutes. To acquire the “external” glycerol value, a sample of the supernatant was added to the glycerol kit, and the OD<sub>540</sub> was measured. For the “internal” measurement, cells in the pellet were washed in 1 ml fresh media that matched the cell media in [NaCl] in order to prevent hypoosmotic shock and internal glycerol leakage during washing. After another flash spin, cells were resuspended in 1 ml fresh media and then incubated, spun, and sampled as described for the “total” glycerol measurement.

### **Saturated Enzymatic Reactions Can Yield Biological Integrators**

Consider a substrate that can be in one of two chemical states: active (e.g., phosphorylated) and inactive (e.g., dephosphorylated). Enzyme  $E_1$  activates the substrate, and enzyme  $E_2$  deactivates the substrate. Under appropriate and often-satisfied conditions (Gomez-Uribe et al., 2007), the rate of change of the concentration of active substrate  $A$  is well approximated by:

$$\frac{dA}{dt} = k_1 \frac{E_1(S_T - A)}{K_1 + E_1 + (S_T - A)} - k_2 \frac{E_2 A}{K_2 + E_2 + A}$$

where  $E_1$  and  $E_2$  are dynamic variables that denote the concentrations of  $E_1$  and  $E_2$ , respectively. The total concentration of substrate is  $S_T$ .  $K_1$  and  $K_2$ , and  $k_1$  and  $k_2$ , are the Michaelis-Menten and catalytic rate constants of  $E_1$  and  $E_2$ , respectively. The canonical Michaelis-Menten rates are a special case of the functions above (which are themselves valid more generally), obtained when the enzyme concentrations  $E_1$  and  $E_2$  are small.

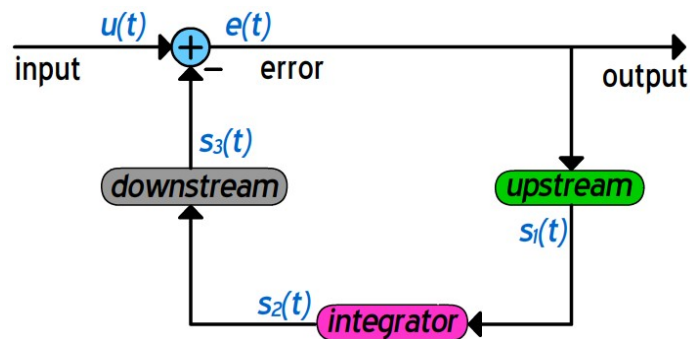
The equation above shows that in general, the rate of change of active substrate concentration depends on the concentration itself. However, when the activation and deactivation reactions are operating in saturating substrate excess (i.e., when  $K_1+E_1 \ll (S_T-A)$ , and  $K_2+E_2 \ll A$ ) then the equation above simplifies to:

$$\frac{dA}{dt} = k_1E_1 - k_2E_2.$$

In such a situation, the rate of change of active substrate is independent of the concentration itself, resulting in a biological integrator, where the dynamics of  $A(t)$  may be obtained simply by integrating the function  $k_1E_1-k_2E_2$  over time. In the main text, we show that there must be one integrating mechanism downstream of Hog1 that requires the kinase activity of Hog1 and is responsible for perfect adaptation in the osmosensing network.

### Quantities Downstream of Integrator Perfectly Adapt, but Those Upstream Do Not

Consider a system with the network schematic shown below, where all the variables represent deviations from the system's rest level (i.e., all the internal variables and the system input are identically zero at rest).



The system has a single input,  $u(t)$ , and a single negative feedback loop containing three subsystems: an integrator and two flanking subsystems called “*upstream*” and “*downstream*” based on their positions relative to the integrator. The error,  $e(t)$ , is the difference between the input  $u(t)$  and  $s_3(t)$ , which is the output of the *downstream* subsystem and the last signal in the feedback loop. The error is the input to the *upstream* subsystem, which has output signal  $s_1(t)$ . The integrator subsystem integrates and potentially scales its input  $s_1(t)$  to generate its output  $s_2(t)$ , which then serves as the input to the *downstream* subsystem.

Assume that the overall system is stable and that a persistent step-input,  $u(t)=u_o$ , is applied at time  $t = 0$ . At steady state, all the signals in the system are constant, and in particular,  $s_1$  must be zero because  $s_2$  is constant and  $s_2$  integrates  $s_1$ . Therefore, the steady-state level of  $s_1$  is independent of the system-input level, and the output of the *upstream* subsystem exhibits perfect adaptation. Now assume that when the steady-state output of the *upstream* subsystem is zero, its steady-state input is identically zero. This assumption is certainly true if the *upstream* subsystem is a stable linear system, but it is true more generally as well (e.g., for nonlinear systems with a single stable steady state). Then, perfect adaptation of  $s_1$  implies perfect adaptation of its input, the error ( $e$ ), which directly implies that the last signal in the loop at steady state is identical to the input, i.e.,  $s_3 = u_o$ . If the *downstream* subsystem is stable and, in particular, has no integrators in it, then its steady-state input  $s_2$  must be nonzero since its steady-state output is nonzero. This argument shows that the signals upstream of the last integrator in the negative feedback loop perfectly adapt, while those downstream of it do not.

The previous example illustrates that integral feedback is sufficient for perfect adaptation of the error and signals upstream of the last integrator. The fact that integral feedback is also necessary for perfect adaptation follows from a more-involved and general derivation, which we do not repeat here (Sontag, 2003; Yi et al., 2000). In this work, we evaluate perfect adaptation in the context of the network diagram in Figure 1B and Figure 4.

### **A Linear Analysis of the Osmosensing Network: Understanding Perfect Adaptation in Terms of Transfer Functions**

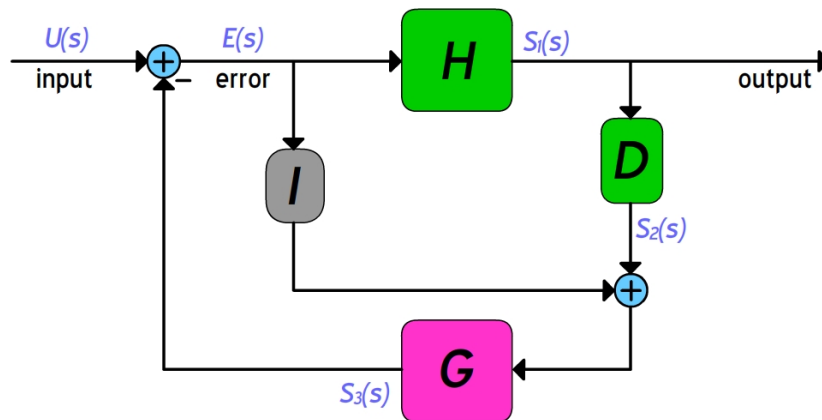
Laplace transforms are very useful when working with linear time-invariant (LTI) systems because analysis that would require calculus can instead be performed using linear algebra. The Laplace transform  $X(s)$  of a function  $x(t)$  is given by

$$X(s) = \int_0^{\infty} x(\tau)e^{-s\tau} d\tau, \text{ where } s \text{ is simply a parameter. An LTI system also can be fully}$$

characterized by a special Laplace transform called the transfer function  $S(s)$  (Oppenheim et al., 1996). The transfer function,  $S(s)$ , of a system relates the Laplace transforms of its input and output via  $Y(s) = S(s)U(s)$ , where  $U(s)$  and  $Y(s)$  are the Laplace transforms of the system input,  $u(t)$ , and output,  $y(t)$ , respectively. By the final-value theorem, for instance, the steady-state input and output are related via  $y_{ss} = S(0)u_{ss}$ , so perfect adaptation of the system output (i.e.,  $y_{ss} = 0$ ) for an LTI system is equivalent to  $S(0) = 0$ , since the input is constant and nonzero.

Using techniques from control engineering, it is a straightforward task to obtain transfer functions for an LTI system from a given network diagram (given the transfer functions of the network's subsystems) or from the set of differential equations

describing the system dynamics (Oppenheim et al., 1996). To most simply understand the implications of our measurements in the osmosensing network, consider an LTI system with the network structure shown below, which is identical to that of the osmosensing network. The transfer function relating the system input to the error in the network is given by  $S_{ue}(s) = \frac{1}{1 + G(DH + I)}$ , where  $G$ ,  $D$ ,  $H$  and  $I$  are the transfer functions of the four subsystems in the network (which we take to be rational functions of polynomials of  $s$ ). Their dependence on the variable  $s$  has been omitted to avoid clutter (i.e., “ $G(s)$ ” is simply written as “ $G$ ”).



Perfect adaptation of the error requires that  $S_{ue}(0)=0$ , which consequently implies that at least one of the four subsystems has a transfer function that goes to infinity (“explodes”) at  $s=0$ . Having a transfer function that explodes at  $s=0$  is equivalent to having one or more integrator(s) within the subsystem, since the transfer function of an integrator is given by  $1/s$ . We can then conclude that perfect adaptation of the error requires that at least one of the four subsystems contains at least one integrator.

Similarly, the transfer function from the system input to measured Hog1 is given by  $S_{us_1}(s) = \frac{H}{1 + G(DH + I)}$ . If  $H(s)$  were the only subsystem performing integration, then Hog1 would not perfectly adapt. One or more of the other subsystems must perform integration (i.e., explode at  $s=0$ ) for Hog1 to perfectly adapt. In the presence of PP1, the connection between Hog1 and the  $D$  subsystem is broken, resulting in the modified transfer function  $S_{us_1}(s) = \frac{H}{1 + GI}$ . Given that Hog1 does not perfectly adapt in this case, we know that the product  $G(s)I(s)$  does not explode at  $s=0$ , which implies that there is no integrator in the series connection of the  $G$  and  $I$  subsystems. Thus, either the  $G$  and  $I$  subsystems both lack integrators, or one subsystem has an integrator but the other itself perfectly adapts. We argue in the Results section that the former is much more likely than the latter. The combination of all our findings points to  $D$  as the subsystem with the last integrator in the feedback loop, the key integrator responsible for perfect adaptation of the error and of Hog1.

Lastly, the transfer function between the system input and glycerol is given by  $S_{us_3}(s) = \frac{G(DH + I)}{1 + G(DH + I)}$ , which shows that as long as there is a single integrator in the feedback loop (i.e., as long as  $G(DH+I)$  explodes at  $s=0$ ), then  $S_{us_3}(0) = 1$ , and the steady-state glycerol will equal the input, producing a steady-state error equal to zero.

## **The Integral of Hog1 Nuclear Enrichment Grows Linearly with Osmostress Magnitude**

Although Hog1 dynamics are nonlinear with respect to the magnitude of the osmostress (e.g., the amplitude saturates; Figure 3A), the time-integral of the Hog1 response increases linearly with the osmostress magnitude (Figure 3D). To see how this latter observation is consistent with integral feedback, suppose that the  $D$  subsystem (Figure 4) is an integrator, as argued in the previous section, and let the other subsystems be potentially nonlinear stable systems without integrators in them. The net change in the output of the  $D$  subsystem in response to a step increase in the system input (i.e., extracellular osmolarity) is precisely the time-integral of Hog1. Two important conclusions follow from assuming that (1) the error perfectly adapts and that (2) the steady-state output of the  $I$  subsystem is zero when its steady-state input (i.e., the error) is zero. First, the stress-induced change in the steady-state input of the  $G$  subsystem simply equals the time-integral of Hog1. Second, the net change in the output of  $G$  (i.e., glycerol) must equal the net change in the system input (i.e., NaCl) in order for the error to go to zero. Thus, the time-integral of Hog1 is directly proportional to the net change in the input of the  $G$  subsystem, and the magnitude of the osmostress is equal to the net change in the output of the  $G$  subsystem. Without loss of generality, suppose that all internal signals measure deviations from their pre-stimulus level. Then the previous argument shows that the steady-state output of the  $G$  subsystem (e.g., the magnitude of the osmostress) equals the steady-state input-output function of the  $G$  subsystem evaluated at a steady-state input proportional to the time-integral of Hog1. If the  $G$  subsystem were perfectly linear, then we would expect that its output would be directly

proportional to its input at steady state, resulting in the time-integral of Hog1 being directly proportional to the magnitude of the osmostress (despite potential nonlinearities in the  $H$  and  $I$  subsystems). This relationship is almost what Figure 3D shows, except that the line relating the integral of Hog1 nuclear enrichment to osmostress magnitude does not cross the origin. This difference may be due to nonlinearities in the input-output steady-state function of subsystem  $G$  that become evident for small ( $< 0.2$  M NaCl) osmostresses.

### Concise Dynamic Model Captures Key Data Features

To certify that our deduced network scenario ( $d$ ) from Figure 4 could recapitulate the key features of our data, we performed quantitative fitting to our Hog1 and glycerol data gathered in the presence and absence of PP1. For simplicity and to minimize parameters, we assumed the system is linear and considered only data gathered for hyperosmotic shocks from 0.0 M to 0.4 M. This restriction neglected some aspects of system behavior (e.g., saturation of Hog1 nuclear enrichment for stronger osmotic shocks; Figure 3A) but still included most important dynamic features. We represented the subsystems as follows:  $H$  and  $G$  as first-order systems,  $I$  as a scalar that multiplies the error, and  $D$  as an integrator. Specifically, we used the following three differential equations with five fit parameters:

$$\frac{d}{dt} \begin{bmatrix} s_1 \\ s_2 \\ s_3 \end{bmatrix} = \begin{bmatrix} -\gamma_h & 0 & -k_h \\ \alpha_d & 0 & 0 \\ 0 & 1 & -(\alpha_i + \gamma_g) \end{bmatrix} \begin{bmatrix} s_1 \\ s_2 \\ s_3 \end{bmatrix} + \begin{bmatrix} k_h \\ 0 \\ \alpha_i \end{bmatrix} u(t)$$

where  $s_1$ ,  $s_2$ , and  $s_3$  are the respective outputs of the  $H$ ,  $D$ , and  $G$  subsystems.  $k_h$  and  $\gamma_h^{-1}$  correspond to the gain and time constant, respectively, of first-order subsystem  $H$ ;  $\alpha_d$  is

the gain of the integrator subsystem  $D$ ;  $\alpha_i$  is the scalar we use to represent subsystem  $I$ , and  $\gamma_g^{-1}$  is the time constant of subsystem  $G$ . The variable  $s_1$  corresponds to our measured Hog1 nuclear enrichment, and the product of  $s_3$  and a sixth fit parameter  $k_g$  corresponds to glycerol measurements. In fitting of data from +PP1 experiments, we set  $\alpha_d = 0$ , and account for decreased efficiency in the import of *hog1-as* by substituting a seventh fit parameter  $k_h'$  for  $k_h$ . For model fitting, we used the *fminsearch* function in Matlab (The Mathworks) with a sum-of-squares cost function; the best-fit parameter values are shown below:

PARAMETER	VALUE
$k_h$	0.496 min <sup>-1</sup>
$k_h'$	0.147 min <sup>-1</sup>
$\gamma_h$	0.369 min <sup>-1</sup>
$\gamma_g$	0.119 min <sup>-1</sup>
$\alpha_i$	0.0806 min <sup>-1</sup>
$k_g$	7.76 min <sup>-1</sup>
$\alpha_d$	0.0106 min <sup>-1</sup>

We conclude from the high-quality fit shown in Figure S8 that network scenario ( $d$ ) from Figure 4 can capture the key features of our data.

## SUPPLEMENTAL REFERENCES

Ferrigno, P., Posas, F., Koepf, D., Saito, H., and Silver, P. (1998). Regulated nucleo/cytoplasmic exchange of HOG1 MAPK requires the importin beta homologs NMD5 and XPO1. *EMBO J* 17, 5606-5614.

Gomez-Urbe, C., Verghese, G., and Mirny, L. (2007). Operating regimes of signaling cycles: statics, dynamics, and noise filtering. *PLoS Comput Biol* 3, e246.

Oppenheim, A., Willsky, A., and Hamid, S. (1996). Signals and Systems, Second edn (Englewood Cliffs, New Jersey: Prentice-Hall).

Sontag, E. (2003). Adaptation and regulation with signal detection implies internal model. *Syst Control Lett* 50, 119-126.

Westfall, P., and Thorner, J. (2006). Analysis of mitogen-activated protein kinase signaling specificity in response to hyperosmotic stress: use of an analog-sensitive HOG1 allele. *Eukaryotic Cell* 5, 1215-1228.

Yi, T., Huang, Y., Simon, M., and Doyle, J. (2000). Robust perfect adaptation in bacterial chemotaxis through integral feedback control. *Proc Natl Acad Sci USA* 97, 4649-4653.

### **Supplemental Figure & Table Legends:**

**Figure S1: Cells with both the *SLN1* and *SHO1* branches intact perfectly adapt on timescale similar to cells lacking the *SHO1* branch.** Response from one representative flow-cell experiment in which cells were shocked with a step input of 0.4M NaCl. The mean of many single cells is shown by the dotted blue line, and three single cells are shown in green, orange, and purple. The shaded region is a band of one standard deviation around the population average and represents the cell-to-cell variability of a single experiment. The Hog1 nuclear enrichment dynamics strongly resemble those shown in Figure 2A.

**Figure S2: Shocked and unshocked cultures have comparable cell-to-cell variability.** Dynamics in single-cell Hog1 nuclear enrichment (shown in green, orange, and purple; defined in Experimental Procedures) and the population average (dark-blue dotted line) measured from a single experiment in which wildtype cells were not osmostressed. The shaded region is a band of one standard deviation around the population average and represents the cell-to-cell variability of a single experiment. This band is comparable in thickness to the one in Figure 2B, where cells were stressed with 0.4 M NaCl. The y-axis scale in this plot is the same as in Figure 2B to facilitate comparison.

**Figure S3: Perfect adaptation of Hog1 nuclear enrichment is not NaCl-specific.** Equivalent hyperosmotic shocks were applied to wildtype cells using one of three common osmolytes: NaCl (0.4 M), KCl (0.4 M), or sorbitol (0.8 M). The maximum

amplitude and dynamics of Hog1 nuclear enrichment were similar across osmolytes, but, most importantly, all three led to perfect adaptation. Error bars represent the standard error of the population average obtained from three independent experiments.

**Figure S4: Cells that retain low-level Hog1 kinase activity can still perfectly adapt.**

A point mutation was introduced into the endogenous *HOG1* gene, which was then YFP tagged at its C-terminus, as in the strains used elsewhere in this study. The point mutation yielded a protein sequence identical to that considered kinase-dead (Ferrigno et al., 1998) but shown later to retain low-level kinase activity (Westfall and Thorner, 2006). The mean, error boundaries, and single-cell plots are as in Figure S1.

**Figure S5: With respect to Hog1 nuclear enrichment and cell volume, PP1 and cycloheximide cause slight deviations compared to untreated cells.**

(A) Cultures from the cell line indicated (e.g., “Wildtype” or “*hog1-as*”) were treated with 100  $\mu\text{g/ml}$  cycloheximide (CHX) or 24  $\mu\text{g/ml}$  PP1, as specified in the legend. Only the dark-blue line corresponds to a culture that was osmostressed, and this trace was included to provide a sense of scale. To obtain a measurement of the osmostress-specific response, the raw +CHX and +PP1 traces shown here were subtracted from the raw response of osmostressed cells. The traces of osmostressed cells corrected in this manner are shown in Figure 5A,B. Dotted lines show the average response, obtained by averaging the population averages from three or four experiments, and the error boundaries depict the standard error of the average response.

(B) Volume traces from the corresponding experiments in (A). As with the traces in (A), the traces here were subtracted from those of osmostressed cells to correct raw volume measurements and obtain the osmostress-specific responses shown in Figure 5C.

**Figure S6: Loss of perfect adaptation in +PP1 cells is not due to nuclear-transport defect.** *hog1-as* cells were grown and loaded into a flow-chamber using media lacking PP1. For five minutes prior to hyperosmotic shock, PP1 was introduced into the flow media. The +PP1 media was then supplemented with 0.4 M NaCl to provide hyperosmotic shock. After 30 minutes, the +NaCl/+PP1 media with replaced by +PP1 media lacking NaCl. Hog1 nuclear enrichment was monitored throughout the experiment. Notably, upon removal of the hyperosmotic stress after 30 minutes, Hog1 exits the nucleus, indicating that *hog1-as* is capable of undergoing nuclear export if hyperosmotic stress is alleviated. The fact that Hog1 nuclear enrichment does not return to its pre-stimulus level could result from the fact that integral feedback is still disrupted by the persistent presence of PP1, and it is only via integral feedback that Hog1 nuclear enrichment can perfectly adapt. Error bars represent the standard error of the population average obtained from three independent experiments.

**Figure S7: Hog1 nuclear enrichment in wildtype cells treated with PP1 still perfectly adapts.** Wildtype cells grown in -NaCl/-PP1 media were loaded into the flow chamber, and then treated with PP1 for five minutes (e.g., -NaCl/+PP1 media) before being hyperosmotically shocked by media with 0.4 M NaCl (e.g., +NaCl/+PP1 media) at  $t = 0$ .

Notably, nuclear enrichment throughout the experiment was diminished relative to –PP1 cells, but perfect adaptation was still intact. Error bars represent the standard error of the population average obtained from three independent experiments.

**Figure S8: Quantitative implementation of deduced network model can recapitulate Hog1 and glycerol dynamics.** Best-fit curves from a model based on network scenario (d) from Figure 4 are shown in purple. Experimental data (Figure 5A,C) is shown in light gray. Panels (A) and (C) show the data and best-fit curves for Hog1 and intracellular glycerol, respectively, in the absence of PP1; panels (B) and (D) are the analogous curves in the presence of PP1. Fit parameters are included in Table S1, and the fitting procedure is described in Supplemental Data. Importantly, model fitting to all four data traces was performed simultaneously.

**Figure S9: Perfect adaptation in Hog1 nuclear enrichment does not require gene expression.** Wildtype cells were loaded into a flow cell in minimal media. The green curve depicts the population mean and standard error (N=3) from experiments in which 100  $\mu$ g/ml cycloheximide was added to the cells five minutes before 0.4 M NaCl entered the flow cell. The trace is corrected for drift in the Hog1 nuclear enrichment in cells not stressed with NaCl (Figure S5). The blue curve illustrates cells that underwent the same osmo-shock but were not treated with cycloheximide.

**Figure S10: Perfect adaptation in Hog1 nuclear enrichment does not require *PFK2*.** The *PFK2* gene was deleted from our *hog1-as* strain, and the cells were exposed to a

hyperosmotic shock with 0.4M NaCl. The dotted blue curve depicts the mean of three independent flow-cell experiments, and the shaded boundary represents the standard error of the mean.

**Figure S11: Comparison of possible calculations of Hog1 nuclear enrichment**

Three metrics for Hog1 nuclear enrichment were used to analyze data from the same flow-cell experiment in which a step input of 0.4M [NaCl] was applied at time 0. The “Total” metric (but not the other two) has been corrected via subtraction of a corresponding “Total” trace from a flow-cell experiment without salt stress. In the absence of this correction, the “Total” trace trends downward over time, since fewer pixels are designated as nuclear when Nrd1-RFP photobleaches. For this reason and others, the “Top-10” and “Average” metrics are more appealing. It may seem counterintuitive that the “Top-10” trace falls below the “Average” trace, but note that the traces above are normalized such that the initial nuclear enrichment is 0 (as described in Experimental Procedures). The “Top-10” metric yields an initial uncorrected value higher than the “Average” metric, so the “Top-10” trace is scaled downward slightly more upon normalization. We favor the “top-10” metric since, even more so than the “average” metric, it is extremely robust to the automated segmentation of nuclear regions whose size changes due to photobleaching.

**Figure S1**

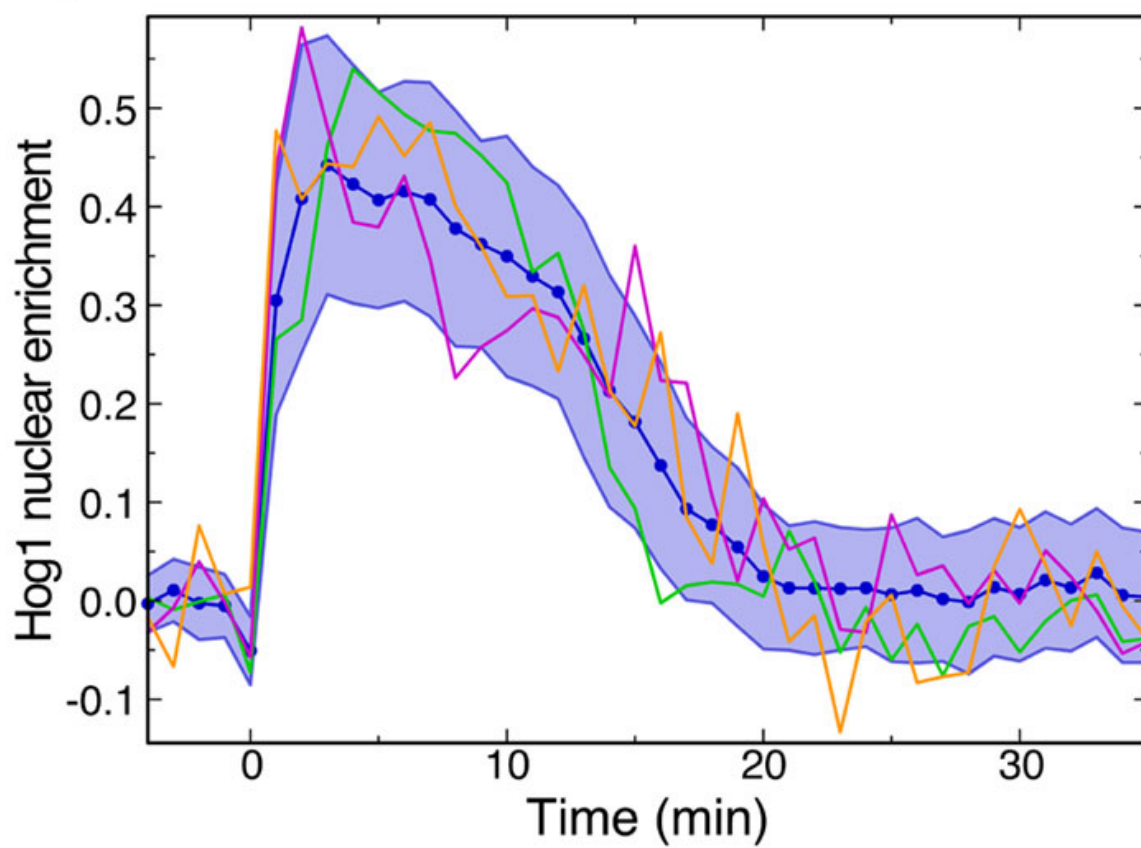


**Figure S2**

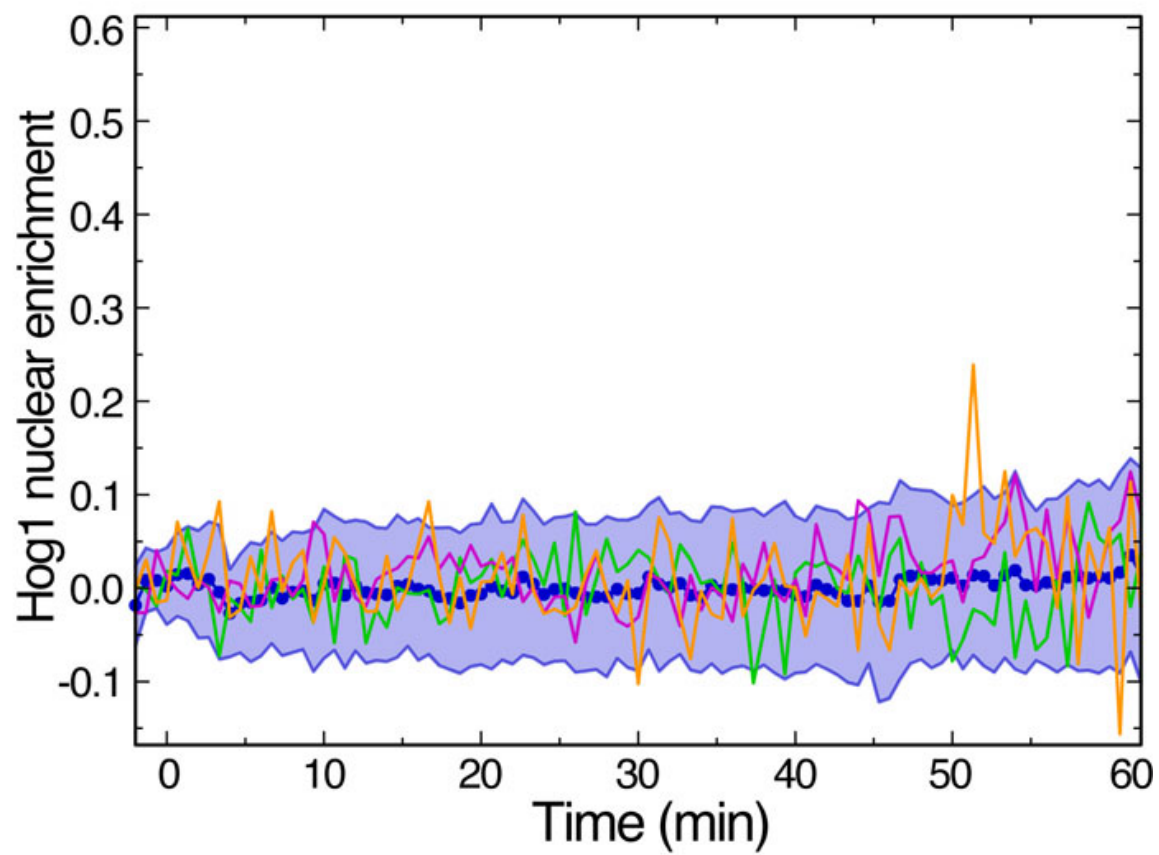


**Figure S3**

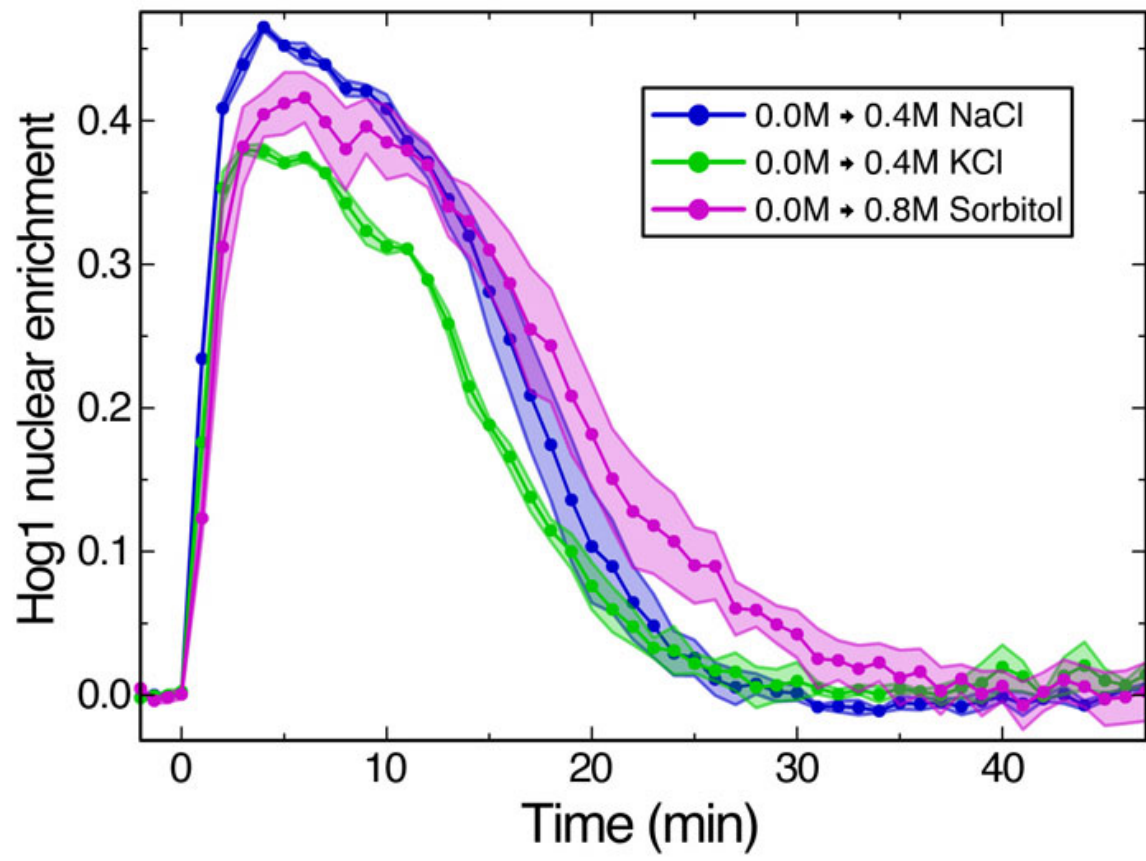


**Figure S4**

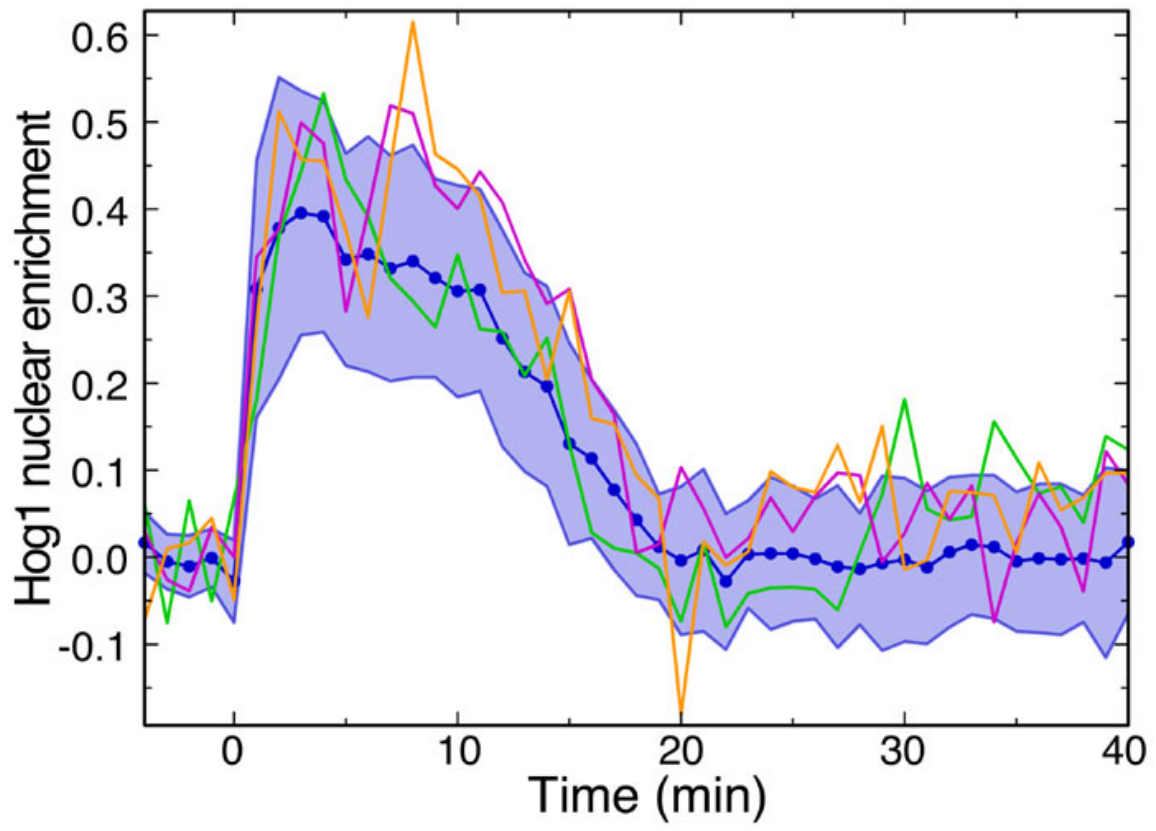


**Figure S5**

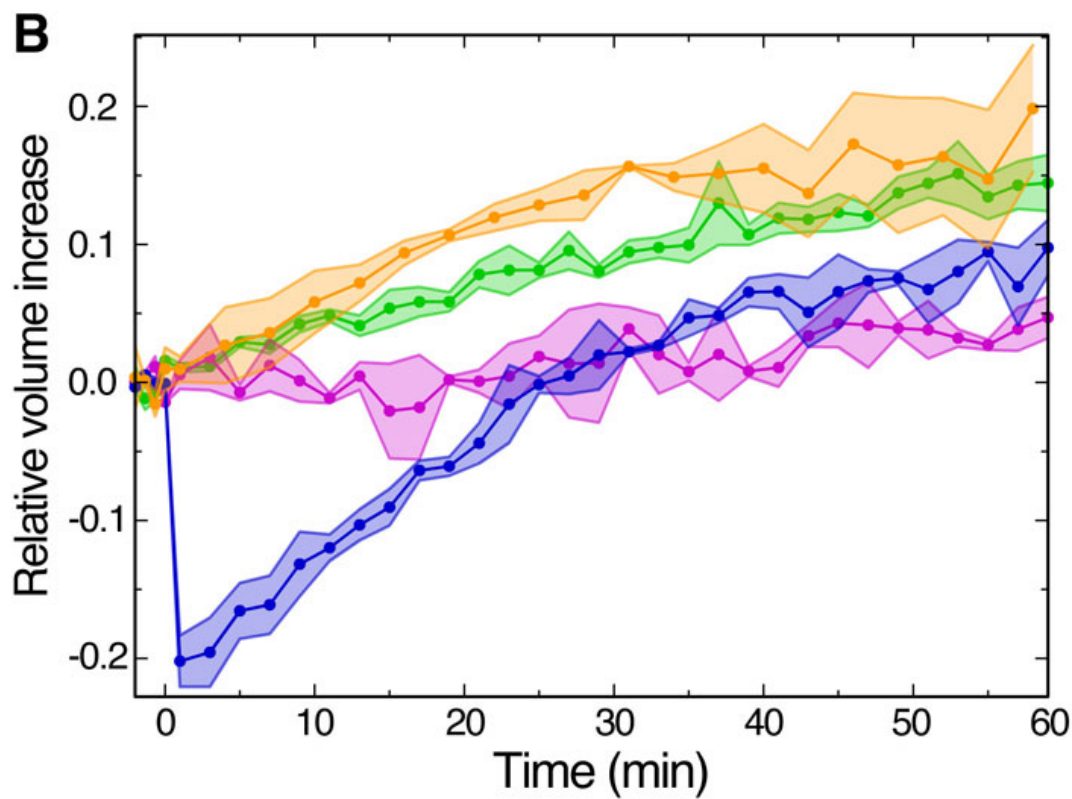
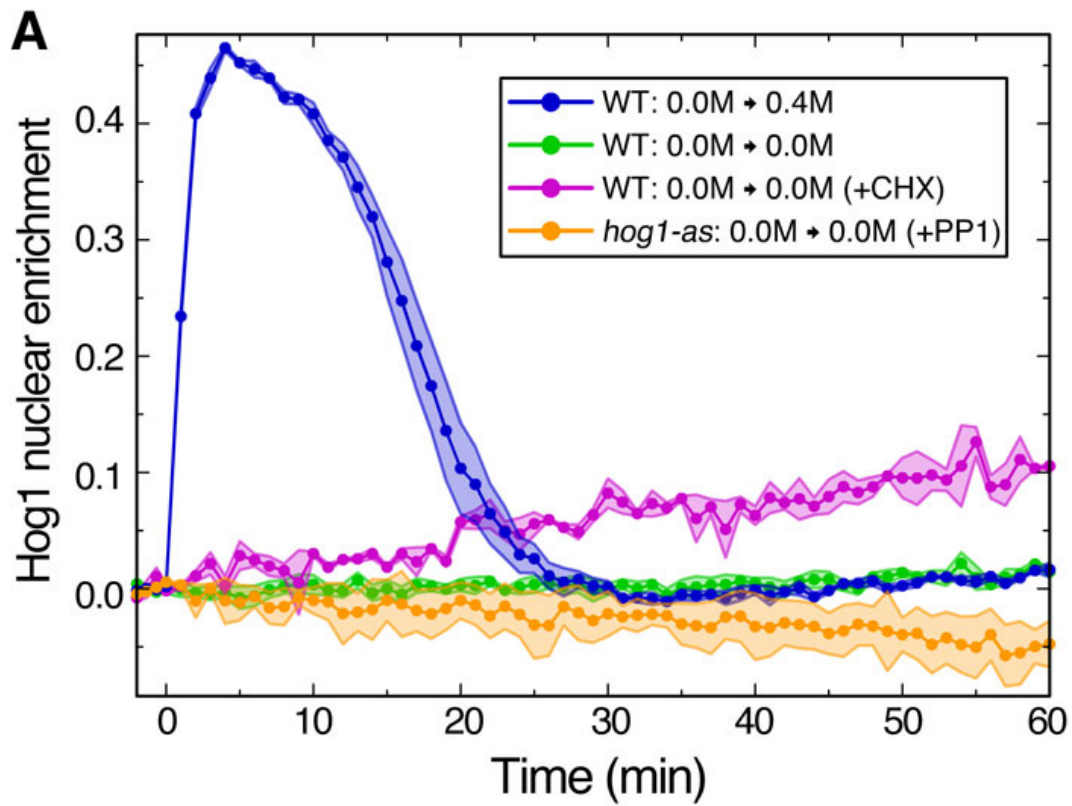


**Figure S6**

[NaCl]: 0.0

0.4

0.0

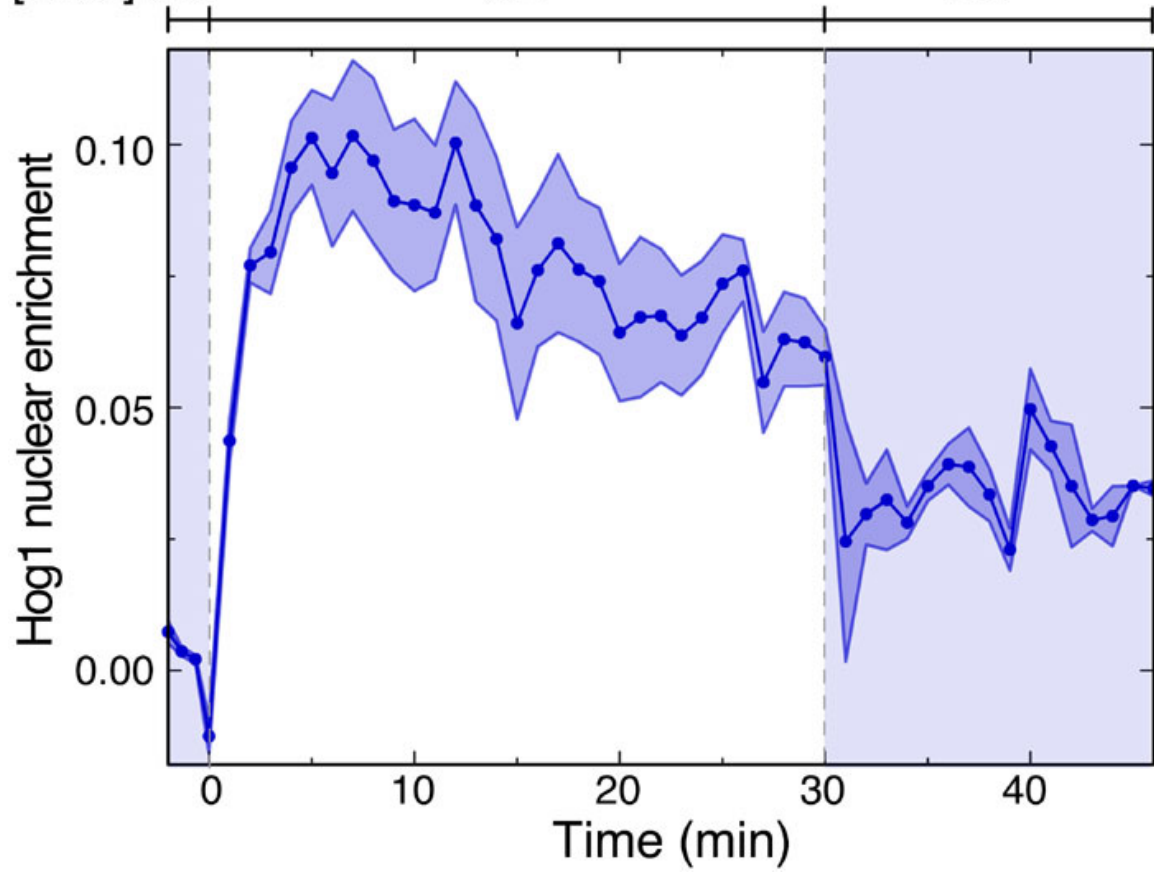
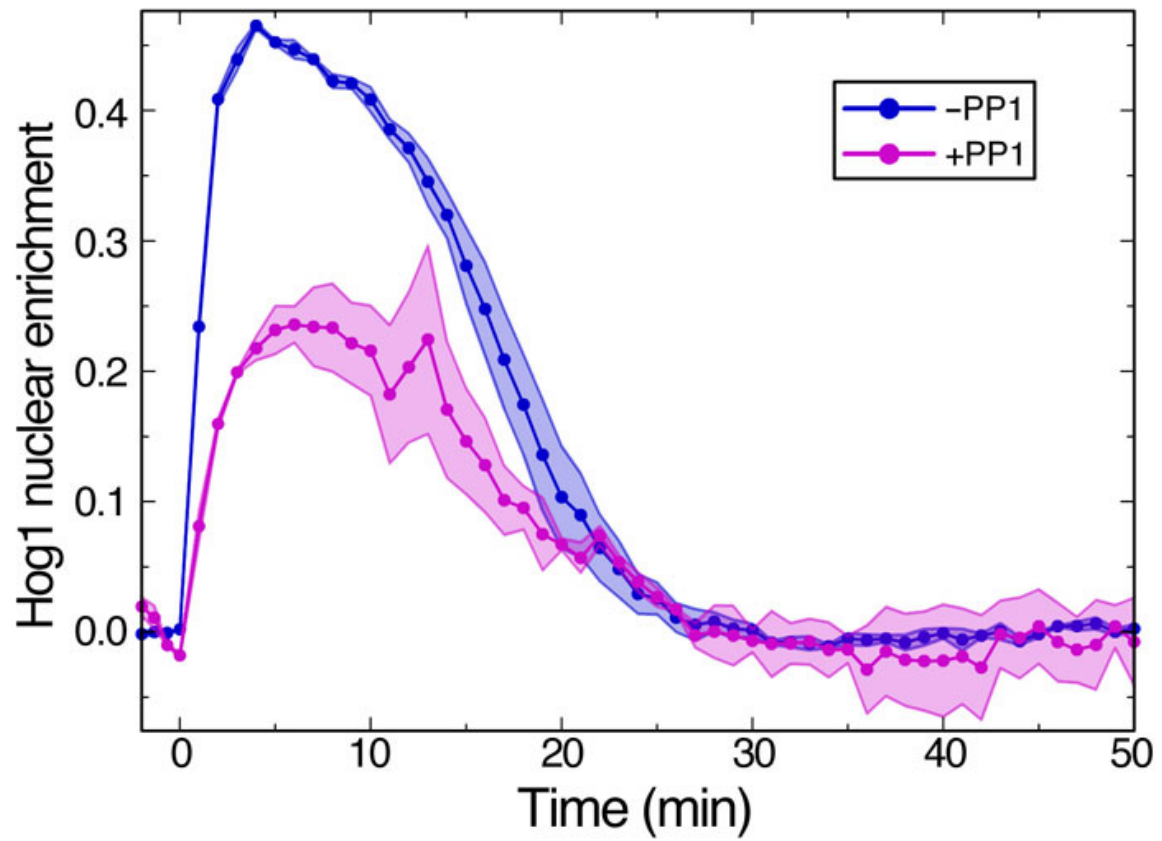
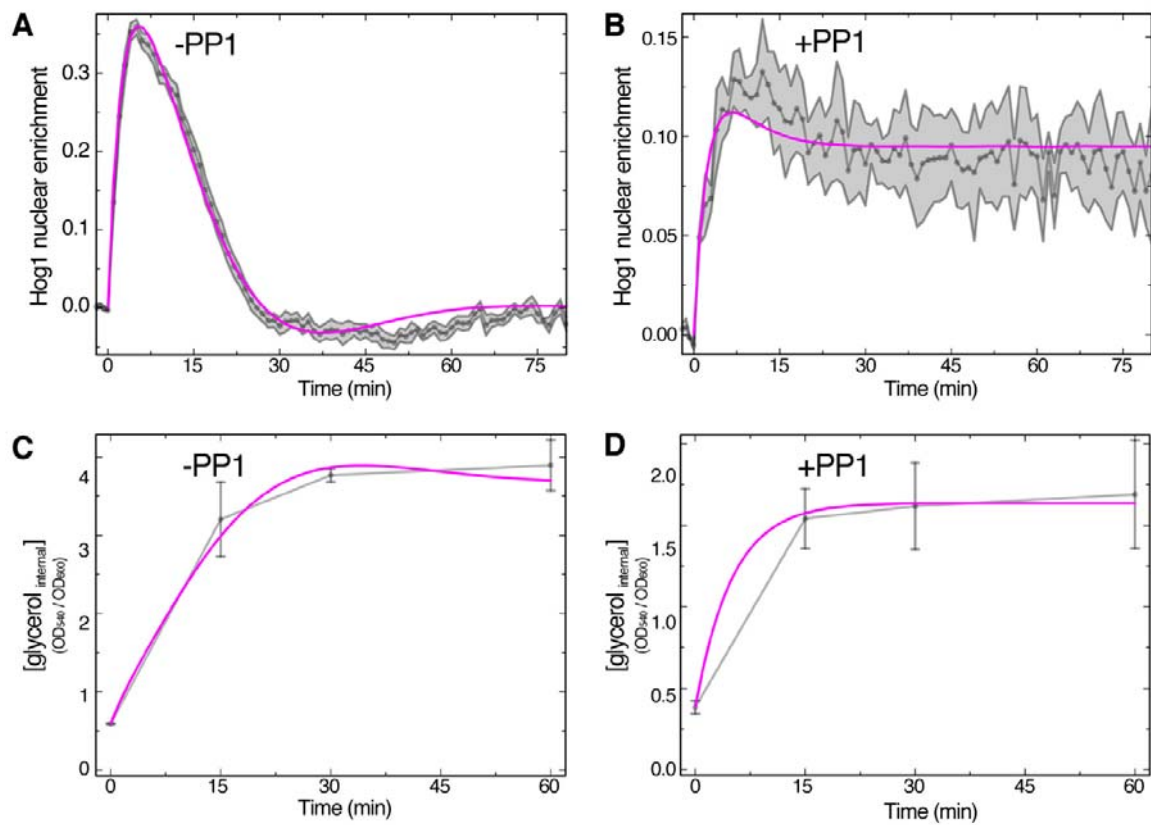


Figure S7



**Figure S8**



**Figure S9**

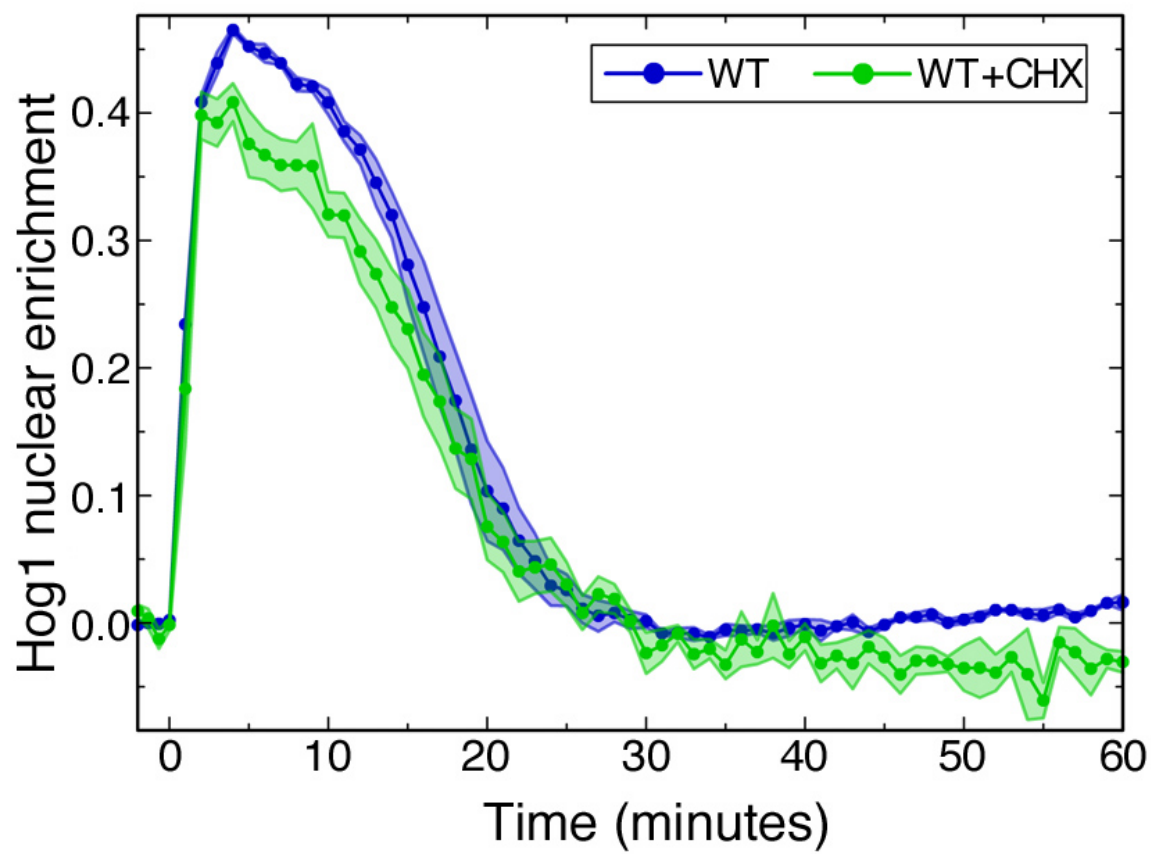


**Figure S10**

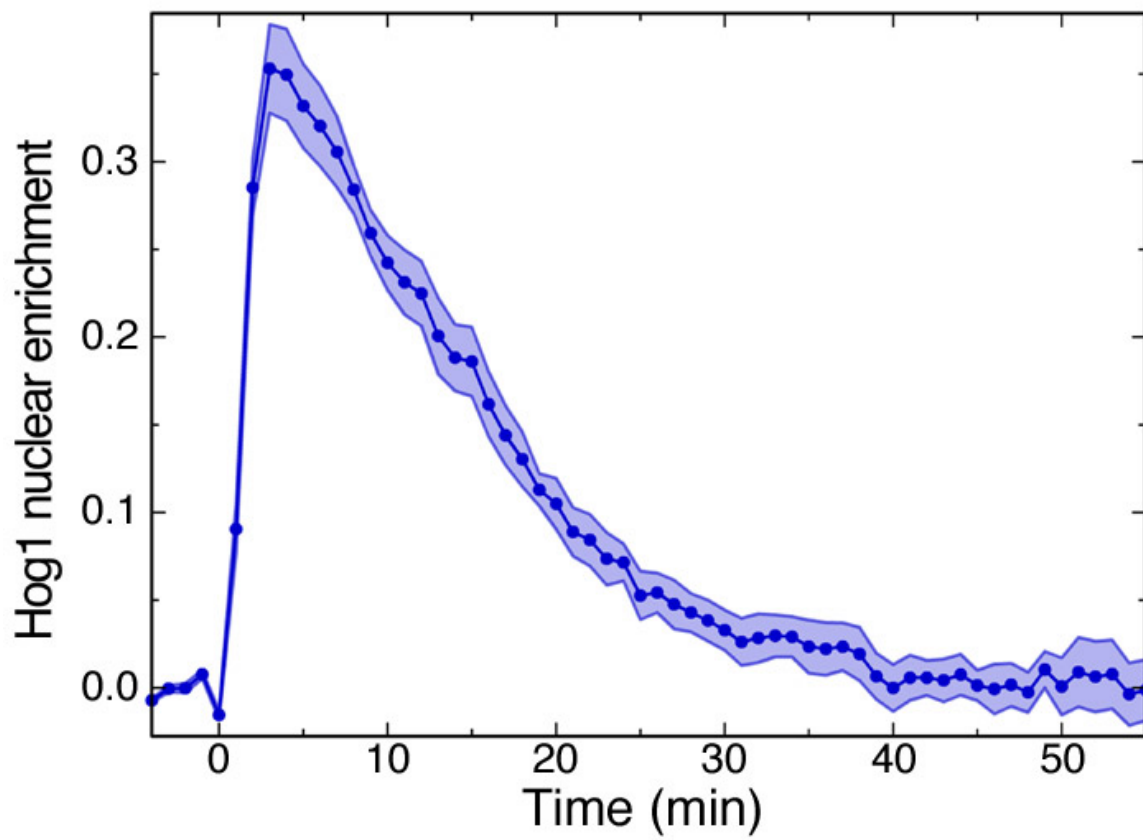


**Figure S11**

